Geophysical Research Letters

RESEARCH LETTER
10.1029/2024GL109348

How P-Wave Scattering Throughout the Entire Mantle Mimics the High-Frequency P_{diff} and Its Coda

Tuo Zhang[1,2], Christoph Sens-Schönfelder[2], Marcelo Bianchi[3], and Klaus Bataille[4]

[1]College of Geophysics, Chengdu University of Technology, Chengdu, China, [2]Section 2.4, Deutsches GeoForschungsZentrum GFZ, Potsdam, Germany, [3]Instituto de Astronomia, Geofísica e Ciências Atmosféricas, Universidade de São Paulo, São Paulo, Brazil, [4]Earth Sciences Department, University of Concepción, Concepción, Chile

Key Points:

- We present observations of high-frequency P_{diff} coda more than 100 s before the core phases even at large distances beyond 150°
- Seismic energy simulations in published models of Earth's mantle heterogeneity show that scattered energy explains P_{diff} and its coda
- Different-depth mantle layers contribute to different time-distance windows of the P_{diff} coda benefiting imaging the mantle heterogeneity

Supporting Information:

Supporting Information may be found in the online version of this article.

Correspondence to:

T. Zhang,
tuo@gfz-potsdam.de

Citation:

Zhang, T., Sens-Schönfelder, C., Bianchi, M., & Bataille, K. (2024). How P-wave scattering throughout the entire mantle mimics the high-frequency P_{diff} and its coda. *Geophysical Research Letters*, *51*, e2024GL109348. https://doi.org/10.1029/2024GL109348

Received 21 MAR 2024
Accepted 20 JUN 2024

Abstract We document the arrival of seismic energy in the core shadow zone up to large distances beyond 150° more than 100 s prior to the core phases. Numerical simulations of the energy transport in an established heterogeneity model show that scattering throughout the entire mantle explains these observations. Diffraction at the core-mantle boundary is unlikely in our 1–2 Hz frequency band and is not required indicating misleading terminology with reference to P_{diff} for the scattered $P*P$-energy. Records of the largest deep earthquakes at low-noise stations are key to the observation of the faint precursory signal which changes appearance with increasing distance from a coda-like decay over a constant amplitude level around 130° to an emergent wave train. According to our simulations, different depth layers in the mantle dominate different time-distance windows of the scattered wave train, providing the opportunity to improve the depth resolution of mantle heterogeneity models.

Plain Language Summary Earthquakes producing different types of waves that travel through the Earth help understand the structure of the Earth. We show that there is seismic energy arriving at stations in the shadow of the Earth's core more than 100 s before the waves usually considered the first arrivals. We used computer simulations to explain how this energy can travel so far in such a short time. Our results show that when there are heterogeneous structures distributed throughout the Earth's mantle the seismic energy can change direction at these structures due to a phenomenon called scattering. This allows the seismic energy to travel in the fast mantle material around the slow Earth's core. Previously, seismologists thought that part of this energy travels along the boundary between core and mantle by a process called diffraction. Our study provides a more elegant explanation for the observed energy and offers new possibilities for the investigation of Earth's structure.

1. Introduction

The traveltime and amplitude of direct phases, like *P*-, *S*-, or surface waves, are routinely used for tomographic imaging of the large-scale structural features (Aki & Lee, 1976; Bozdağ et al., 2016; Lei et al., 2020; Li & van der Hilst, 2010; Simmons et al., 2021; Zhu et al., 2012) showing that Earth exhibits different levels of anomalous structure from the lithosphere down to the deep mantle of the Earth. Most prominently the two large low-shear-velocity provinces (LLSVPs) above the Core-Mantle Boundary (CMB) have been identified (Lay et al., 1998; Ni et al., 2002) with major consequences for Earth's dynamic processes and the thermal and chemical evolution of the mantle (French & Romanowicz, 2015; Garnero, 2004; Koelemeijer et al., 2017; Maruyama et al., 2007).

Additionally to the main seismic phases, there is energy that is observed but not predicted by spherically symmetric or even state-of-the-art deterministic 3D Earth models. It originates from 3D structure at scales below the resolution limits of current imaging techniques. This small-scale structure is of distinct importance for the investigation of geodynamic processes as it carries information about chemical heterogeneities (Cormier et al., 2023, e.g. phase changes) that can exist over longer times than thermal heterogeneity even on small scales. Wave interaction with the small-scale structure deforms the shape of the ballistic arrivals (Zheng & Wu, 2008) and generates scattered waves which then arrive in partially unexpected time-distance windows. Usually, such scattered waves follow the main seismic phases in seismograms and were first investigated by Aki (1969) and termed *seismic coda*. Seismologists observed coda waves following the direct wave arrivals but also found scattered energy arriving before some direct phases forming a *precursor* to a seismic phase. Scattered energy is most prominently observed in short-period seismograms: *P* coda (Aki, 1973), P_{diff} coda (Bataille et al., 1990; Husebye & Madariaga, 1970), *PP* precursors (Bolt et al., 1968), *P′P′* precursors (Earle et al., 2011), *PKP*

precursors (J. Cleary & Haddon, 1972) and *PKiKP* coda (Vidale & Earle, 2000) are prominent examples of scattered phases at teleseismic distances (Shearer, 2015). However, despite the abundance of scattered energy in teleseismic records the distribution of heterogeneity in the deep Earth required to explain these observations is a field of active research.

PKP precursors are energy that precedes the *PKP* arrival by up to 20 s in the distance range from 120° to 145°. This early arrival of energy is facilitated by the deflection of *PKPab* and *PKPbc* waves into this distance range that would otherwise not be accessible for these phases. Scattering by small-scale heterogeneity near the CMB was suggested as the cause (J. Cleary & Haddon, 1972; Haddon & Cleary, 1974; Hiemer & Thomas, 2022). Later, some studies interpreted the *PKP* precursor as a result of scattering that happened throughout the whole mantle (Hedlin et al., 1997; Mancinelli & Shearer, 2013; Margerin & Nolet, 2003).

A similar precursory signal in the distance range 155°–170° was observed by Sens-Schönfelder et al. (2021). However, this precursor originates from the scattering of *PKPbc* and is only seen above 4 Hz when the earlier arriving *PKIKP* phase is attenuated in the Inner Core. Precursory signals are especially useful for the investigation of heterogeneity since these waves are not affected by the main arrival which usually has much larger amplitude. However, the number of precursory signals is small, limiting the information that can be obtained about the location of heterogeneity. The depth sensitivity of the nearly vertically propagating *PKP* precursors, for instance, does not provide strong constraints about the depth extent of heterogeneity. The existence of small-scale heterogeneity in the whole mantle agrees with results obtained from stacked *PP* precursor signals (Bentham et al., 2017) which are thought to originate from scattering in the crust and uppermost mantle (J. R. Cleary et al., 1975; King et al., 1975) or possibly the middle mantle (Rost et al., 2008).

The strong small-scale heterogeneity in the near-surface is regarded as the main cause of the *P* coda (Aki, 1973; Dainty, 1990). However, synthetic models of scattering in the whole mantle also fit global stacks of teleseismic *P* coda (Shearer & Earle, 2004). With the epicentral distance increasing above ≈100°, the core shadow inhibits the arrival of direct *P* waves at the surface. Diffraction along the CMB, however, generates the P_{diff} phase which allows waves to propagate with mantle velocities to longer distances into the core shadow. The diffraction process is most effective at long wavelength and diminishes at high frequencies (Rost et al., 2006). Besides the diffracted waves, the waves passing through the core for example, *PKP* constitute the first arriving energy in long-period recording beyond 100° distances. Bataille and Lund (1996) observed that the ratio between the amplitudes of the ballistic phase and the coda changes drastically during the transition from *P* to P_{diff}. Therefore, P_{diff} coda was suggested to originate from multiple scattering near the CMB (Bataille et al., 1990; Tono & Yomogida, 1996). A more detailed investigation of P_{diff} coda was conducted by Earle and Shearer (2001). Their global stacking of short-period recordings for P_{diff} coda extends to epicentral distances of 130°. They modeled the observation with single-scattering theory but considered small-scale heterogeneity throughout the whole mantle with P_{diff} coda being generated by scattering of both *P* and P_{diff}. However, from the analysis of data from the Canadian Yellowknife Array, Rost et al. (2006) conclude that P_{diff} does not propagate to distances larger than about 108° at frequencies around 1 Hz.

These differing models show that there is no consensus about the location of the heterogeneity that generates the P_{diff} coda. Here we try to reconcile these observations and clarify the relationship between the origin of energy observed in the P_{diff} coda time window and the *P*-wave diffraction. We focus on the signal following the P_{diff} arrival time with the new observation of P_{diff} coda at high frequencies covering a large distance range, reaching beyond 150° in stacked records of largest-magnitude very deep global earthquakes. We simulate synthetic seismogram envelopes with an existing heterogeneity model (Earle & Shearer, 2001) to interpret the origin of the high-frequency P_{diff} and its coda.

2. Observation

For the investigation of P_{diff} coda, we select the frequency band 1–2 Hz since it provides the best signal-to-noise ratio in accordance with earlier studies. The epicentral distance range is chosen from 70° to 160°. We select earthquakes with magnitude ≥7.9 M_w from the years 1994–2021 resulting in 52 events. For each event, vertical-component data is downloaded from all available stations in the IRIS and GFZ-GEOFON archives, instrument-corrected, detrended and filtered in the 1–2 Hz band. Seismogram envelopes are computed using the Hilbert-Transform and smoothed twice by computing a moving average with time windows of 2.5 and 8 s length.

10.1029/2024GL109348

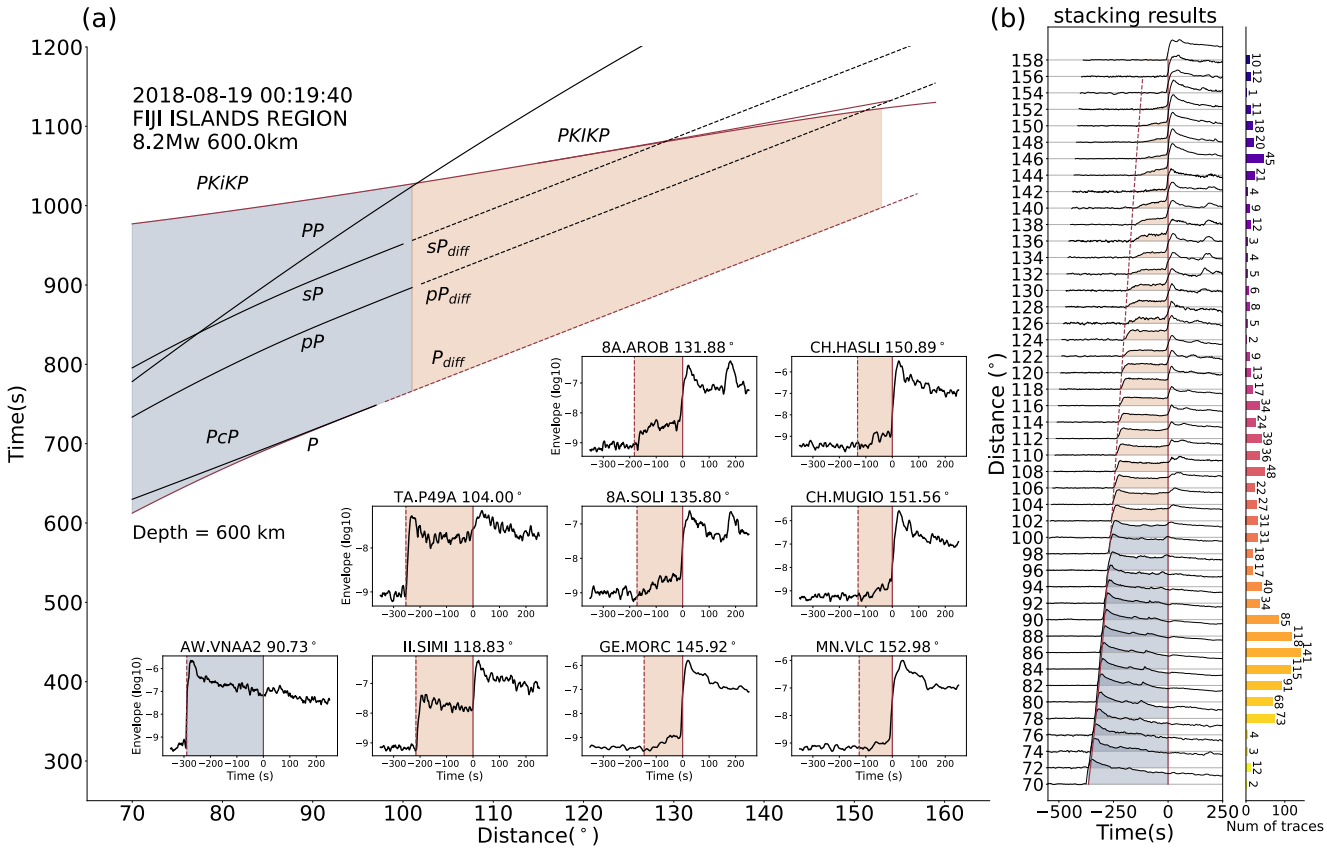

Figure 1. (a) Theoretical arrival times of seismic phases from a 600-km depth earthquake calculated with the ak135 model. The time window between the arrival time of *P* or P_{diff} and *PKiKP* or *PKIKP* phases which are investigated here is indicated by color shading. For distances larger than 102° the core phase is the earliest arrival as it overtakes the *PP* arrival. Insets show logarithmic envelopes of single station vertical records from the 600 km deep M_w 8.2 event that occurred on 19 August 2018, in the Fiji Islands region. Traces are aligned to the earliest arriving core phase (*PKiKP* or *PKIKP*). (b) Stacked traces for this event. *P* or P_{diff} coda is highlighted by shading in the time window corresponding to (a). The number of traces used in the stacks is shown on the right.

Figure 1a shows the theoretical arrival times of seismic phases calculated by ObsPy/TauP (Crotwell et al., 1999; Krischer et al., 2015) from a 600-km deep earthquake in the ak135 velocity model (Kennett et al., 1995) together with processed envelopes from the 600-km-deep 8.2 M_w event which occurred on 19 August 2018, in the Fiji Islands region. Traces are aligned to the arriving time of the earliest core phase (*PKiKP* for pre-critical distances and *PKIKP* for post-critical distances). In accordance with common naming conventions we define the *P* coda or P_{diff} coda as the waves following the theoretical arrival time of the *P* or P_{diff} phases, respectively. At short distances, for example, 70°–102° the *P* coda window (gray area) contains scattered *P* waves together with coda waves or precursors of *pP*, *sP*, *PcP* and *PP* phases. In the core shadow beyond 102° *PKiKP* or *PKIKP* should become the first arrival since P_{diff} does not propagate beyond 108° at these frequencies (Rost et al., 2006). However, scattered *P*-energy can arrive in the 200 s long P_{diff} coda window (orange area). This energy has been studied up to 130° distance by Earle and Shearer (2001). The constituents of this intermediate P_{diff} coda window are also manifold. It may contain scattered *P*, *pP*, *sP* or P_{diff} energy but also precursors of *PP* and *PKP*. The frequently studied *PKP* precursor starts at 120° in this distance range, but it precedes the *PKP* arrival by up to 20 s, only, whereas the P_{diff} coda starts more than 100 s prior to *PKP*. At even larger distances the energy in the P_{diff} coda window can be detected in individual seismograms even more than 150° away from the epicenter preceding the core phase by more than 100 s. This is regularly observed also for other events as illustrated by Figure S1 in Supporting Information S1.

Since global stacking significantly improves the signal-to-noise ratio of retrieved envelopes we processed records from 52 events (Supporting Information S1). Figure 1b shows the best event, the 19 August 2018 Fiji Islands region earthquake. In Supporting Information S1, we show stacked envelopes for two shallow, one intermediate-depth, and two other deep events. We detect the P_{diff} coda in all events including stations located at very long

distances ($\Delta > 150°$) but largest deep focus events provide the clearest signal due to weaker crustal scattering on the source side.

This dependence on the absolute signal level together with the frequency-magnitude distribution means that a stack of different earthquakes is unlikely to be better than the record of the best event alone. Another reason why we use the events individually is that the shape of traces from the shallow and deep events are different due to the arrival times of the *pP*, *sP*, and *PP* phases, especially at shorter distances. Consequently, we study individual events and focus here on the Fiji Island event to study the P_{diff} coda.

3. Modeling

3.1. Models of Whole Earth Scattering

Spherically symmetric models of the Earth have been proposed based on the main teleseismic phases for example, PREM (Dziewonski & Anderson, 1981), iasp91 (Kennett, 1991) or ak135-F (Kennett et al., 1995; Montagner & Kennett, 1996). More precise 3D Earth models have been derived more recently, like SPiRaL (Simmons et al., 2021). The macroscopic elastic structure is intrinsically averaged over the resolution length of the applied tomographic method. Small-scale heterogeneity, that is, structure at the spatial scale below the resolution length can be described statistically based on random medium theory (Sato et al., 2012). It uses the power spectral density function (PSDF) of the parameter fluctuations (e.g., wave velocity or density) as a description of the heterogeneity. The PSDF is the Fourier transform of the autocorrelation function (ACF) which is characterized by the correlation length a and the amplitude ε of the small-scale perturbations.

Small-scale structures in the Earth can exist in the crust, mantle or inner core. In the liquid outer core, small-scale heterogeneity is assumed to be erased quickly by convection. Lateral variations of heterogeneity and attenuation in the shallow Earth have a strong influence on the high-frequency seismic wavefield (Calvet et al., 2013; P. Gaebler et al., 2019; P. J. Gaebler et al., 2015; Mayor et al., 2016; Sens-Schönfelder et al., 2009; van Dinther et al., 2020), especially in volcanic areas (Carcolé & Sato, 2010; De Siena et al., 2016).

Deep Earth scattering is mostly investigated using the *PKP* precursors. The heterogeneity near the CMB that causes the single-scattering energy to arrive earlier at the surface than the ballistic minimax phase *PKPab* and explains the observation of precursors to *PKP* (J. Cleary & Haddon, 1972; Haddon & Cleary, 1974). Scattering in the whole mantle was invoked to explain the shape of the *PKP* precursor (Hedlin et al., 1997; Mancinelli & Shearer, 2013; Margerin & Nolet, 2003). Whole mantle scattering was also used to explain the P_{diff} coda (Earle & Shearer, 2001) and *P* coda (Shearer & Earle, 2004). Bentham et al. (2017) developed a model to fit the observation of globally stacked *PP* precursors in the distance range from 70° to 120° which includes heterogeneity in the lithosphere and three different layers in the mantle. The heterogeneity parameters of these models are shown in Figure 2c.

3.2. Monte Carlo Simulation

We model the propagation of scattered energy using the Monte Carlo simulations of the 3D radiative transfer equations in a spherically symmetric Earth model at 1 Hz (Sens-Schönfelder et al., 2021). Figure 2b shows snapshots of the energy field from Monte Carlo simulations with and without 3D multiple elastic scattering using the ES2001 heterogeneity model (Earle & Shearer, 2001). The 600 km deep isotropic source is located at the right side (black star) of the snapshots taken at 1,020 s. Simulations in the heterogeneous model show smoother energy distributions compared to the homogeneous model. Energy filling the space between the main seismic phases is generated by scattering off the heterogeneity. Arrows indicate the location of P_{diff} coda observations at the epicentral distance of 150°, where energy has already arrived at the illustrated at 1,020 s lapse time in the heterogeneous model while no energy has reached the receiver in the model without scattering.

We compare the observation of the Fiji event with the synthetics from four rather simplistic models of deep Earth heterogeneity in Figure 2a. The SE2004 model is not able to reproduce the shape of the P_{diff} coda. The simulated envelopes of the H1997 and BRT2017 models agree reasonably well with the shape of the P_{diff} coda but show an increase of energy after *PKiKP* or *PKIKP* phase that is not observed in the data. Although this time window is not the focus of our study, it indicates a discrepancy, which might be caused by unsuitable scattering patterns of the mantle with correlation length $a = 8$ km. Envelopes of the ES2001 model fit the observations best.

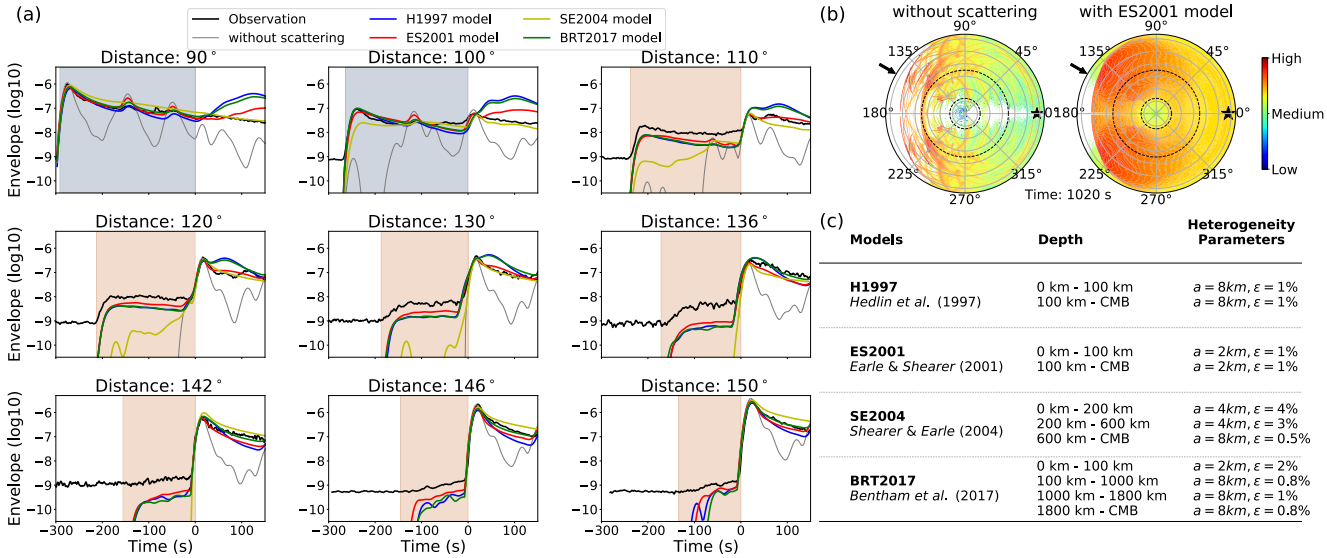

Figure 2. (a) Observed (solid black curves) and synthetic seismogram envelopes with heterogeneity in the four models given in (c) and without any heterogeneity (gray curves). Shadings correspond to Figure 1a. (b) Cross sections of the Monte Carlo simulation without scattering and with 3D multiple nonisotropic scattering using the ES2001 model at lapse time 1,020 s. The color indicates the logarithm of the seismic energy. The arrow indicates the epicentral distance of 150° where energy is only present at this lapse time due to heterogeneity. (c) Table of four 1D spherically symmetric models of Earth heterogeneity.

4. Discussion

4.1. Origin of P_{diff} and Its Coda

In accordance with previous work, we refer to the energy arriving between P_{diff} and *PKIKP* as P_{diff} *coda*. This terminology avoids ambiguity with the term *PKP precursor* used for the energy arriving a few seconds before *PKP* at distances 120° < Δ < 145°. Early interpretations of P_{diff} coda suggested it originates from multiple scattering near the CMB in the D" layer (Bataille et al., 1990). This process would be rather similar to diffraction that generates P_{diff} but would be more effective at high frequencies (Bataille & Lund, 1996). With the scattering of the whole mantle proposed to interpret the *PKP* precursors (Hedlin et al., 1997), Earle and Shearer (2001) proposed the single-scattering modes like *P*-to-*P*, P_{diff}-to-*P* or *P*-to-P_{diff} originating in the whole mantle to generate the P_{diff} coda. However, Rost et al. (2006) reported that P_{diff} is not detectable at large distances in the short-period wavefield. We investigated the contribution of diffraction using a combination of our scattering simulations with analytic propagation along the CMB resulting in the contribution from the deflection of diffracted waves that is small compared to the contribution of scattering (Supporting Information S1).

To investigate which depth range contributes to the scattered energy in the different time windows, we designed a number of single-layer heterogeneity models based on the ES2001 model in which scattering can only occur in one particular layer. The results are shown in Figure 3. Each curve indicates the result from one single-layer heterogeneity model with color indicating the depth of the scattering layer.

Figure 3 shows that at distances for example, 90°, the *P* coda is dominated by scattering at the lithospheric heterogeneity (dark blue curve). At the 100°, P_{diff} and its coda appear instead of *P*. By design, the Monte Carlo simulation does not model the diffraction process but still matches the 1 Hz observation of what is usually referred to as the diffracted P_{diff}. The energy creating the onset at the P_{diff} arrival time originates from scattering in the lower mantle (orange lines) with a simultaneous onset of all curves at about −250 s resulting in a strong peak reproducing the apparent P_{diff} arrival and its early coda. Note that there is no energy at this time in the simulation without scattering, yet (gray curve). The peaks at −150 s and −100 s that are also present without scattering represent the ballistic depth phases *pP* and *sP*.

With distance increasing to 120°, energy arriving from different layers separates and arrives at different times. Deeper layers contribute to earlier arrivals while the later part of the P_{diff} coda stems from the shallower layers. All layers of the mantle contribute to P_{diff} coda in this distance range but with varying contributions at different travel times. As a consequence the peak at the P_{diff} arrival time decreases in amplitude and the decay of its coda is

10.1029/2024GL109348

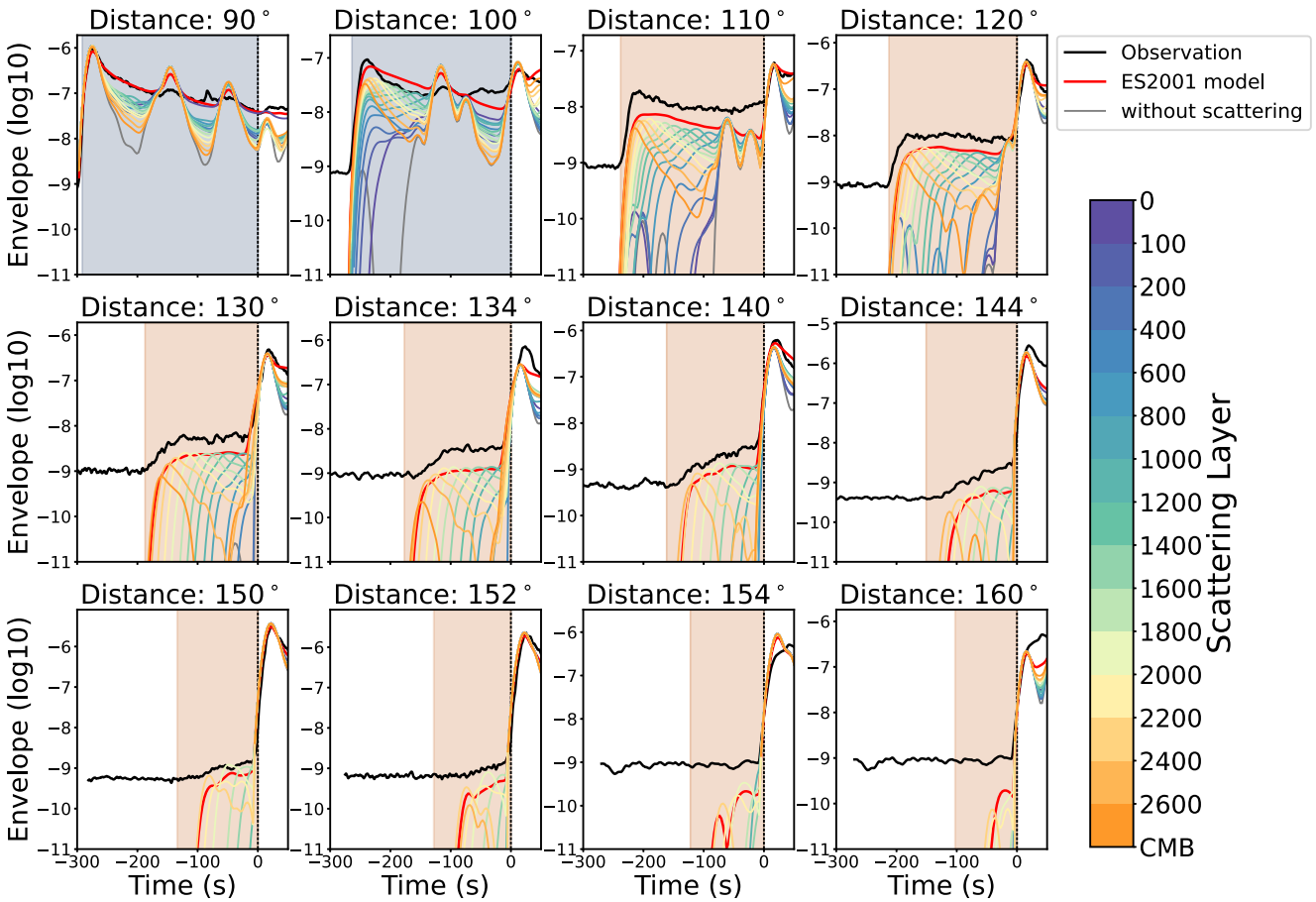

Figure 3. Simulation results from single-layer heterogeneity models based on the ES2001 model. Colors correspond to the depth of each scattering layer according to the colorbar. Observations (black curves), the simulation without any scattering (gray curves) and the simulation of scattering in the full ES2001 model (red curves) are shown for comparison.

reduced toward larger distances. This explains the observation of decreasing peak amplitude with increasing distance (Bataille & Lund, 1996; Earle & Shearer, 2001). What is usually referred to as P_{diff} at high frequencies is not diffracted but actually scattered energy mostly originating from the lowermost mantle. It should therefore better be called P_{scatt} or $P*P$.

When the distance increases above 130° no P_{diff} arrival can be observed anymore. Decreasing amplitude of the P_{diff} arrival with increasing distance would also be expected if diffraction was important. However, in this case also the coda of the P_{diff} phase would vanish. Instead there is a gradual increase of energy toward the P_{diff} coda and the onset time depends on the noise conditions of the observing station. Earliest energy which is scattered close to the CMB decreases in amplitude (orange curves) and assumes a notable delay compared to the theoretical P_{diff} arrival. Both, the gradual increase of the envelope and the delay of the coda onset can be readily observed in the data. The increase shortly before the *PKIKP* peak at intermediate distances originates from the scattering of core phases in deep layers, as expected for the *PKP* precursor.

Close to 150°, the P_{diff} coda emerges from the noise with an almost linear increase in the logarithmic plots in Figure 3. The observed slope is well reproduced by the model. Energy arriving in this time-distance window can only originate from scattering in the middle mantle about 2,000 km deep (yellow curve) as deeper *single*-scattering cannot propagate energy around the core to these distances. At 160° and beyond, the scattered energy is very weak and not observed in the seismograms since it is below the noise level even at the best stations.

From this modeling, we conclude that P_{diff} and P_{diff} coda at frequencies above 1 Hz constitute energy scattered by heterogeneity in the mantle at different depths. This is the same heterogeneity that is also responsible for the generation of the *PP* precursor and coda. Different depths contribute to different lapse times of the coda

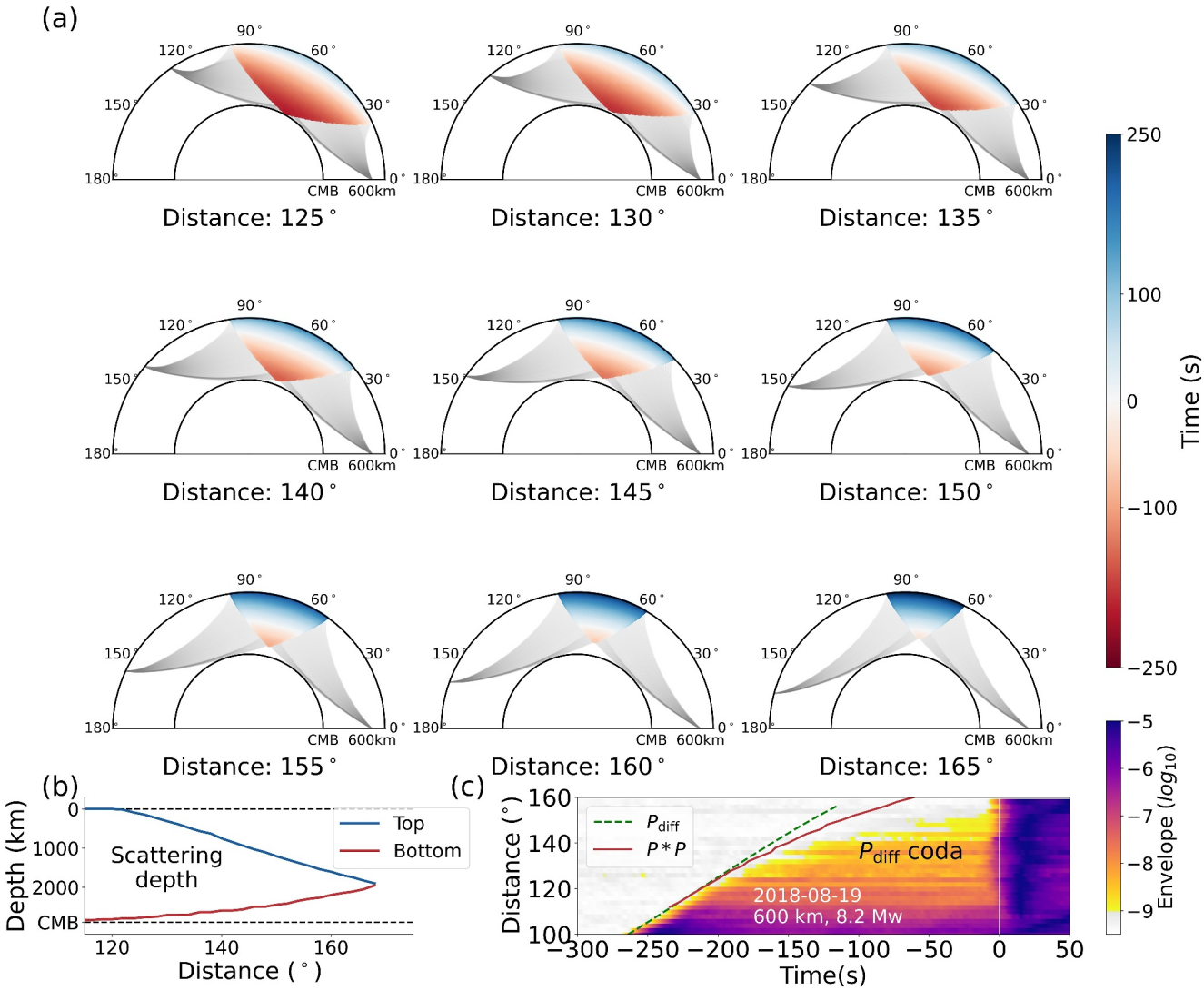

Figure 4. (a) Cross sections through the great circle plane of all possible single-scattering positions (the colored areas) for different epicenter distances. The color indicates travel times resulting from single scattering. Times are aligned to the arrival time of the *PKIKP* phase at each distance. Red represents the location contributing to P_{diff} coda with arrival times before *PKIKP*. Energy scattered in the blue areas arrives after *PKIKP*. (b) Depth range contributing to the P_{diff} coda. Blue curve shows the upper limit given by top of the red regions in (a). The bottom of the possible single-scattering locations for each distance is shown in red. Both approach each other in the middle mantle at about 2,000 km depth for an epicentral distance of 168°. (c) The earliest possible time (onset time) of single scattering energy (red curve) at each distance compared with the theoretical arrival time of P_{diff} (dashed green curve) and the observed P_{diff} coda energy (color shading).

generating the variable shapes of P_{diff} and P_{diff} coda at different distances. No diffraction is involved in the propagation of this energy.

To illustrate the regions in which scattering can contribute to the P_{diff} coda, Figure 4a shows possible travel paths of P_{diff} coda for nine different distances. The colored areas indicate potential locations of single scattering ($P*P$) in the great circle plane with color encoding the resulting arrival time at the station. The time is aligned to the arrival time of the *PKIKP* phase at each distance such that the red area indicates the scattering region that contributes the P_{diff} coda while scattering in the blue regions leads to arrivals later than *PKIKP*. As the distance increases, the boundary between red and blue regions shifts from shallow depth toward the deep Earth indicating that the large distance observations of P_{diff} coda rely on mid to lower mantle scattering. Meanwhile, a shadow zone above the CMB starts to appear for single-scattering. Scattering close to the CMB (e.g., in D") cannot contribute to the P_{diff} coda at distances larger than ≈150° anymore. Consequently, the region in which single scattering can generate P_{diff} coda narrows toward larger distances. The upper limit lowers to maintain short travel

times and the lower limit rises for the energy to pass around the core as illustrated in Figure 4b. Beyond 168° no P_{diff} coda can be generated by single scattering anymore as confirmed by the observations (Figure 3).

We calculate the earliest possible time of single-scattered energy at each distance and compare it to the observed P_{diff} onset in Figure 4c. There is a time lag between the theoretical P_{diff} arrival and the predicted onset of single scattering energy which increases with distance to about 30 s at 150°. Observations follow the predicted single scattering onset more closely than the theoretical P_{diff} arrival time.

We stress that the simulations in the ES2001 model predict the shape of the P_{diff} coda even at 150° rather well (Figure 3). This confirms that scattering is an important process in the generation of this signal whereas P wave diffraction appears to have a minor effect. We suggest two possible explanations for the relative underestimation of the P_{diff} coda level (Figure 2a) (I): increased attenuation of core phases and (II): a remaining effect of diffraction. Selective attenuation of core phases in a layer close to the CMB would not affect the scattered P waves but lead to a relative increase in comparison to the core phases (Figure S5 in Supporting Information S1). Short-range diffraction would enlarge the regions in which scattering can contribute to the P_{diff} coda and potentially increase its energy (Figure S6 in Supporting Information S1).

4.2. Relation to Earlier Work

Our model-based interpretation of the P_{diff} and P_{diff} coda signals as scattered waves with insignificant contribution of CMB diffraction is in line with Earle and Shearer (2001). They used stacks of shallower events with magnitudes down to $M_w = 5.7$ to observe P_{diff} coda up to a distance of 130°, only and interpret it as scattered energy. However, Earle and Shearer (2001) invoke a contribution of diffraction. Rost et al. (2006) on the other hand report on the basis of a comparable data set analyzed with beamforming that P_{diff} is not observed at distances larger than 108°.

Our modeling reconciles these seemingly contradictory observations. Volumetric scattering of P waves does not only explain P_{diff} coda, it also explains the early onset in the core shadow, that is, P_{diff} itself. The large volume in which scattering can occur to shed energy in the early P_{diff} time window leads to a broadening of the slowness range such that the scattered energy will be filtered out by beamforming applied by Rost et al. (2006). Also the P_{diff} coda will be filtered out by the array processing due to the wide slowness range. This underlines our finding that high-frequency energy arriving in the time window between the theoretical arrival of P_{diff} and the core phases is not diffracted, but scattered by heterogeneity distributed in the whole mantle.

This effect is similar to the observations of the $PKP - Cdiff$ phase and its coda at high frequencies (Adam & Romanowicz, 2015; Tanaka, 2005). This phase has been interpreted as being diffracted around the inner core boundary but can be explained by scattering due to the presence of heterogeneity in the mantle (Sens-Schönfelder et al., 2021). In both cases ($PKP - Cdiff$ and P_{diff}) diffraction might play a role but is not sufficient to explain the observations. On the other hand there is consensus about scattering in the mantle and independently derived models of mantle heterogeneity can explain the key features of observed signals.

5. Conclusions

We have for the first time observed the P_{diff} coda at high frequencies of 1–2 Hz at an epicentral distance of more than 150°. The stacking of global earthquake envelopes shows that this signal is best observed for the deepest earthquakes with the largest magnitudes. Global stacks of high-SNR P_{diff} coda envelopes of the 600 km deep 8.2 M_w 2018 Fiji Islands event are compared to Monte Carlo simulations of 3D scattering in published 1D spherically symmetric heterogeneity models. The new observations are reasonably well predicted by the synthetic envelopes which fit the different shapes of P_{diff} and its coda in the different distance ranges that transition from an apparent arrival with decaying coda over constant energy to an emergent signal. Different depth layers contribute to energy arriving at different times in the P_{diff} coda providing a new opportunity to investigate the depth distribution of heterogeneity. This is an interesting perspective to complement PKP precursor observations which provide limited depth constraints.

High-frequency P_{diff} is dominantly generated by the same process as the P_{diff} coda. The lowermost-mantle scattering contributes to the earliest part of P_{diff} coda that used to be recognized as P_{diff} when the distance is not too large. With the scattering layer rising toward later lapse times, the energy arrival is dominated by one depth layer after the other which causes the P_{diff} coda to be devoid of the typical coda decrease. The depth range

contributing to the generation of the P_{diff} coda narrows toward larger epicentral distance (≥130°). Both, the lowermost mantle and uppermost mantle may not contribute to P_{diff} coda at long distances. Beyond 168° distance the possibility to propagate energy into the P_{diff} coda by single scattering vanishes completely.

In conclusion, we argue that what is usually referred to as P_{diff} and its coda at high frequencies is an expression of P wave scattering by heterogeneity distributed throughout the Earth mantle without any significant contribution of diffraction. It constitutes another precursor to the core phases rather than coda and should consequently be referred to as P_{scatt} or $P*P$. This scattering process is also responsible for the generation of the PP precursor and will affect all ballistic phases that propagate through the mantle. The underlying heterogeneity is not restricted to the D"-layer close to the CMB or to the lithosphere. Our analysis supports the presence of moderate small-scale heterogeneity throughout the entire mantle.

Data Availability Statement

All seismic data are freely available and can be downloaded from the GEOFON data centre of the GFZ German Research Centre for Geosciences (https://geofon.gfz-potsdam.de) and the Incorporated Research Institutions for Seismology Web Services (https://service.iris.edu/). The links for downloading the data from the networks are given in Supporting Information S1 (Tables S1–S6) with the station information.

Acknowledgments
This study was supported by the National Natural Science Foundation of China (42304075) and the Deutsche Forschungsgemeinschaft (DFG, German Research Foundation)—521548357. The authors thank the Editor, Daoyuan Sun and two reviewers, Vernon Cormier and an anonymous reviewer for their constructive comments and suggestions that helped us to improve the manuscript.

References

Adam, J.-C., & Romanowicz, B. (2015). Global scale observations of scattered energy near the inner-core boundary: Seismic constraints on the base of the outer-core. *Physics of the Earth and Planetary Interiors*, *245*, 103–116. https://doi.org/10.1016/j.pepi.2015.06.005

Aki, K. (1969). Analysis of the seismic coda of local earthquakes as scattered waves. *Journal of Geophysical Research*, *74*(2), 615–631. https://doi.org/10.1029/JB074i002p00615

Aki, K. (1973). Scattering of p waves under the Montana Lasa. *Journal of Geophysical Research*, *78*(8), 1334–1346. https://doi.org/10.1029/JB078i008p01334

Aki, K., & Lee, W. H. K. (1976). Determination of three-dimensional velocity anomalies under a seismic array using first p arrival times from local earthquakes: 1. A homogeneous initial model. *Journal of Geophysical Research*, *81*(23), 4381–4399. https://doi.org/10.1029/JB081i023p04381

Bataille, K., & Lund, F. (1996). Strong scattering of short-period seismic waves by the core-mantle boundary and the p-diffracted wave. *Geophysical Research Letters*, *23*(18), 2413–2416. https://doi.org/10.1029/96GL02225

Bataille, K., Wu, R., & Flatte, S. (1990). Inhomogeneities near the core-mantle boundary evidenced from scattered waves: A review. *Pure and Applied Geophysics*, *132*(1), 151–173. https://doi.org/10.1007/BF00874361

Bentham, H., Rost, S., & Thorne, M. (2017). Fine-scale structure of the mid-mantle characterised by global stacks of pp precursors. *Earth and Planetary Science Letters*, *472*, 164–173. https://doi.org/10.1016/j.epsl.2017.05.027

Bolt, B. A., O'Neill, M., & Qamar, A. (1968). Seismic waves near 110°: Is structure in core or upper mantle responsible? *Geophysical Journal International*, *16*(5), 475–487. https://doi.org/10.1111/j.1365-246X.1968.tb02310.x

Bozdağ, E., Peter, D., Lefebvre, M., Komatitsch, D., Tromp, J., Hill, J., et al. (2016). Global adjoint tomography: First-generation model. *Geophysical Journal International*, *207*(3), 1739–1766. https://doi.org/10.1093/gji/ggw356

Calvet, M., Sylvander, M., Margerin, L., & Villaseñor, A. (2013). Spatial variations of seismic attenuation and heterogeneity in the Pyrenees: Coda q and peak delay time analysis. *Tectonophysics*, *608*, 428–439. https://doi.org/10.1016/j.tecto.2013.08.045

Carcolé, E., & Sato, H. (2010). Spatial distribution of scattering loss and intrinsic absorption of short-period S waves in the lithosphere of Japan on the basis of the Multiple Lapse Time Window Analysis of Hi-net data. *Geophysical Journal International*, *180*(1), 268–290. https://doi.org/10.1111/j.1365-246X.2009.04394.x

Cleary, J., & Haddon, R. (1972). Seismic wave scattering near the core-mantle boundary: A new interpretation of precursors to PKP. *Nature*, *240*(5383), 549–551. https://doi.org/10.1038/240549a0

Cleary, J. R., King, D. W., & Haddon, R. A. W. (1975). P-Wave scattering in the Earth's crust and upper mantle. *Geophysical Journal International*, *43*(3), 861–872. https://doi.org/10.1111/j.1365-246X.1975.tb06200.x

Cormier, V. F., Lithgow-Bertelloni, C., Stixrude, L., & Zheng, Y. (2023). Mantle phase changes detected from stochastic tomography. *Journal of Geophysical Research: Solid Earth*, *128*(2), e2022JB025035. https://doi.org/10.1029/2022JB025035

Crotwell, H. P., Owens, T. J., & Ritsema, J. (1999). The TauP Toolkit: Flexible seismic travel-time and ray-path utilities. *Seismological Research Letters*, *70*(2), 154–160. https://doi.org/10.1785/gssrl.70.2.154

Dainty, A. M. (1990). Studies of coda using array and three-component processing. *Pure and Applied Geophysics*, *132*(1–2), 221–244. https://doi.org/10.1007/BF00874364

De Siena, L., Calvet, M., Watson, K., Jonkers, A., & Thomas, C. (2016). Seismic scattering and absorption mapping of debris flows, feeding paths, and tectonic units at Mount St. Helens volcano. *Earth and Planetary Science Letters*, *442*, 21–31. https://doi.org/10.1016/j.epsl.2016.02.026

Dziewonski, A. M., & Anderson, D. L. (1981). Preliminary reference Earth model. *Physics of the Earth and Planetary Interiors*, *25*(4), 297–356. https://doi.org/10.1016/0031-9201(81)90046-7

Earle, P. S., Rost, S., Shearer, P. M., & Thomas, C. (2011). Scattered P'P' observed at short distances. *Bulletin of the Seismological Society of America*, *101*(6), 2843–2854. https://doi.org/10.1785/0120110157

Earle, P. S., & Shearer, P. M. (2001). Distribution of fine-scale mantle heterogeneity from observations of P_{diff} coda. *Bulletin of the Seismological Society of America*, *91*(6), 1875–1881. https://doi.org/10.1785/0120000285

French, S. W., & Romanowicz, B. (2015). Broad plumes rooted at the base of the earth's mantle beneath major hotspots. *Nature*, *525*(7567), 95–99. https://doi.org/10.1038/nature14876

Gaebler, P., Eken, T., Bektaş, H. O., Eulenfeld, T., Wegler, U., & Taymaz, T. (2019). Imaging of shear wave attenuation along the central part of the North Anatolian Fault Zone, Turkey. *Journal of Seismology*, *23*(4), 913–927. https://doi.org/10.1007/s10950-019-09842-1

Gaebler, P. J., Sens-Schönfelder, C., & Korn, M. (2015). The influence of crustal scattering on translational and rotational motions in regional and teleseismic coda waves. *Geophysical Journal International*, *201*(1), 355–371. https://doi.org/10.1093/gji/ggv006

Garnero, E. J. (2004). A new paradigm for earth's core-mantle boundary. *Science*, *304*(5672), 834–836. https://doi.org/10.1126/science.1097849

Haddon, R., & Cleary, J. (1974). Evidence for scattering of seismic PKP waves near the mantle-core boundary. *Physics of the Earth and Planetary Interiors*, *8*(3), 211–234. https://doi.org/10.1016/0031-9201(74)90088-0

Hedlin, M. A., Shearer, P. M., & Earle, P. S. (1997). Seismic evidence for small-scale heterogeneity throughout the earth's mantle. *Nature*, *387*(6629), 145–150. https://doi.org/10.1038/387145a0

Hiemer, V., & Thomas, C. (2022). Generation of reflections and PKP precursors from a scattering layer in d. *Geophysical Research Letters*, *49*(4), e2021GL096900. https://doi.org/10.1029/2021GL096900

Husebye, E., & Madariaga, R. (1970). The origin of precursors to core waves. *Bulletin of the Seismological Society of America*, *60*(3), 939–952. https://doi.org/10.1785/BSSA0600030939

Kennett, B. L. N. (1991). Iaspei 1991 seismological tables. *Terra Nova*, *3*(2), 122. https://doi.org/10.1111/j.1365-3121.1991.tb00863.x

Kennett, B. L. N., Engdahl, E. R., & Buland, R. (1995). Constraints on seismic velocities in the Earth from traveltimes. *Geophysical Journal International*, *122*(1), 108–124. https://doi.org/10.1111/j.1365-246X.1995.tb03540.x

King, D., Haddon, R., & Husebye, E. (1975). Precursors to. *Physics of the Earth and Planetary Interiors*, *10*(2), 103–127. https://doi.org/10.1016/0031-9201(75)90029-1

Koelemeijer, P., Deuss, A., & Ritsema, J. (2017). Density structure of earth's lowermost mantle from Stoneley mode splitting observations. *Nature Communications*, *8*(1), 1–10. https://doi.org/10.1038/ncomms15241

Krischer, L., Megies, T., Barsch, R., Beyreuther, M., Lecocq, T., Caudron, C., & Wassermann, J. (2015). Obspy: A bridge for seismology into the scientific python ecosystem. *Computational Science & Discovery*, *8*(1), 014003. https://doi.org/10.1088/1749-4699/8/1/014003

Lay, T., Williams, Q., & Garnero, E. J. (1998). The core–mantle boundary layer and deep earth dynamics. *Nature*, *392*(6675), 461–468. https://doi.org/10.1038/33083

Lei, W., Ruan, Y., Bozdağ, E., Peter, D., Lefebvre, M., Komatitsch, D., et al. (2020). Global adjoint tomography—Model GLAD-M25. *Geophysical Journal International*, *223*(1), 1–21. https://doi.org/10.1093/gji/ggaa253

Li, C., & van der Hilst, R. D. (2010). Structure of the upper mantle and transition zone beneath Southeast Asia from traveltime tomography. *Journal of Geophysical Research*, *115*(B7), B07308. https://doi.org/10.1029/2009JB006882

Mancinelli, N. J., & Shearer, P. M. (2013). Reconciling discrepancies among estimates of small-scale mantle heterogeneity from PKP precursors. *Geophysical Journal International*, *195*(3), 1721–1729. https://doi.org/10.1093/gji/ggt319

Margerin, L., & Nolet, G. (2003). Multiple scattering of high-frequency seismic waves in the deep earth: PKP precursor analysis and inversion for mantle granularity. *Journal of Geophysical Research*, *108*(B11) 2514. https://doi.org/10.1029/2003JB002455

Maruyama, S., Santosh, M., & Zhao, D. (2007). Superplume, supercontinent, and post-perovskite: Mantle dynamics and anti-plate tectonics on the core–mantle boundary. *Gondwana Research*, *11*(1), 7–37. https://doi.org/10.1016/j.gr.2006.06.003

Mayor, J., Calvet, M., Margerin, L., Vanderhaeghe, O., & Traversa, P. (2016). Crustal structure of the Alps as seen by attenuation tomography. *Earth and Planetary Science Letters*, *439*, 71–80. https://doi.org/10.1016/j.epsl.2016.01.025

Montagner, J.-P., & Kennett, B. L. N. (1996). How to reconcile body-wave and normal-mode reference earth models. *Geophysical Journal International*, *125*(1), 229–248. https://doi.org/10.1111/j.1365-246X.1996.tb06548.x

Ni, S., Tan, E., Gurnis, M., & Helmberger, D. (2002). Sharp sides to the African superplume. *Science*, *296*(5574), 1850–1852. https://doi.org/10.1126/science.1070698

Rost, S., Garnero, E. J., & Williams, Q. (2008). Seismic array detection of subducted oceanic crust in the lower mantle. *Journal of Geophysical Research*, *113*(B6), B06303. https://doi.org/10.1029/2007JB005263

Rost, S., Thorne, M. S., & Garnero, E. J. (2006). Imaging global seismic phase arrivals by stacking array processed short-period data. *Seismological Research Letters*, *77*(6), 697–707. https://doi.org/10.1785/gssrl.77.6.697

Sato, H., Fehler, M. C., & Maeda, T. (2012). *Seismic wave propagation and scattering in the heterogeneous Earth*. Springer Science & Business Media. https://doi.org/10.1007/978-3-642-23029-5

Sens-Schönfelder, C., Bataille, K., & Bianchi, M. (2021). High-frequency (6 Hz) PKPab precursors and their sensitivity to deep Earth heterogeneity. *Geophysical Research Letters*, *48*(2), e2020GL89203. https://doi.org/10.1029/2020GL089203

Sens-Schönfelder, C., Margerin, L., & Campillo, M. (2009). Laterally heterogeneous scattering explains LG blockage in the Pyrenees. *Journal of Geophysical Research*, *114*(B7), B07309. https://doi.org/10.1029/2008JB006107

Shearer, P. M. (2015). 1.24—Deep Earth structure: Seismic scattering in the deep Earth. In G. Schubert (Ed.), *Treatise on geophysics* (2nd ed., pp. 759–787). Oxford: Elsevier. https://doi.org/10.1016/B978-0-444-53802-4.00018-X

Shearer, P. M., & Earle, P. S. (2004). The global short-period wavefield modelled with a Monte Carlo seismic phonon method. *Geophysical Journal International*, *158*(3), 1103–1117. https://doi.org/10.1111/j.1365-246X.2004.02378.x

Simmons, N. A., Myers, S. C., Morency, C., Chiang, A., & Knapp, D. R. (2021). SPiRaL: A multiresolution global tomography model of seismic wave speeds and radial anisotropy variations in the crust and mantle. *Geophysical Journal International*, *227*(2), 1366–1391. https://doi.org/10.1093/gji/ggab277

Tanaka, S. (2005). Characteristics of PKP-CDIFF coda revealed by small-aperture seismic arrays: Implications for the study of the inner core boundary. *Physics of the Earth and Planetary Interiors*, *153*(1), 49–60. https://doi.org/10.1016/j.pepi.2005.05.007

Tono, Y., & Yomogida, K. (1996). Complex scattering at the core-mantle boundary observed in short-period diffracted p-waves. *Journal of Physics of the Earth*, *44*(6), 729–744. https://doi.org/10.4294/jpe1952.44.729

van Dinther, C., Margerin, L., & Campillo, M. (2020). Laterally varying scattering properties in the North Anatolian Fault Zone from ambient noise cross-correlations. *Geophysical Journal International*, *225*(1), 589–607. https://doi.org/10.1093/gji/ggaa606

Vidale, J. E., & Earle, P. S. (2000). Fine-scale heterogeneity in the Earth's inner core. *Nature*, *404*(6775), 273–275. https://doi.org/10.1038/35005059

Zheng, Y., & Wu, R. (2008). Theory of transmission fluctuations in random media with a depth-dependent background velocity structure. In *Advances in Geophysics, Earth heterogeneity and scattering effects on seismic waves* (Vol. 50, pp. 21–41). Elsevier. https://doi.org/10.1016/S0065-2687(08)00002-2

Zhu, H., Bozdağ, E., Peter, D., & Tromp, J. (2012). Structure of the European upper mantle revealed by adjoint tomography. *Nature Geoscience*, *5*(7), 493–498. https://doi.org/10.1038/ngeo1501